Optical Materials 109 (2020) 110259

Contents lists available at ScienceDirect

Optical Materials

journal homepage: http://www.elsevier.com/locate/optmat

Invited Article

Combined optical-electrical modeling of perovskite solar cell with an optimized design

T. Bendib [a,b,*], H. Bencherif [c,d], M.A. Abdi [b,c], F. Meddour [b,c], L. Dehimi [e,f], M. Chahdi [b,f]

[a] Faculty of Technology, University of M'sila, 28000, Algeria
[b] LEPCM, University of Batna 1, 05000, Algeria
[c] Faculty of Technology, University of Batna 2, 05000, Algeria
[d] LAAAS, Department of Electronics, University Batna 2, Algeria
[e] LMSM, University of Biskra, Biskra, Algeria
[f] Faculty of Science, University of Batna 1, 05000, Algeria

ARTICLE INFO

Keywords:
Perovskite solar cell
SCAPS-1D
Transfer matrix
Optical modeling
Design optimization
Conversion efficiency

ABSTRACT

This paper deals with the investigation of an optimized design of n-i-p perovskite solar cell by means of combined optical and electrical approach. The proposed approach is mainly based on Transfer Matrix Method (TMM) and SCAPS-1Dsimulator. It considers different optical and electrical mechanisms. Several electron and hole transport proprieties are examined to enhance the solar cell efficiency. The proposed approach permits to balance the compromise between high optical performance and good band alignment for ETM and HTM candidates. The obtained results show that tin dioxide (SnO_2) and Zinc oxide (ZnO) are appropriates candidates as ETL materials. Concerning the HTL materials, the suggested Nickel (II) oxide (NiO) is the appropriate one. The optimized design with ZnO as ETM and NiO as HTM outperforms the conventional solar cell in terms of short circuit current density by (23.84 mA/cm^2), open circuit voltage by (1.268 V), fill factor and efficiency by (83.77%) and (24.94) respectively. Hence, the proposed approach is definitely practical not just for investigating perovskite solar cells' high-efficiency, but also for implementation in SCAPS-1D software, in order to precisely examine and optimize different solar cells optical and electrical performance.

1. Introduction

Third generation perovskite-based photovoltaic technologies have proved outstanding evolution in conversion of solar energy since their first employment in 2009 [1]. Owing to their superior and adjustable electro-optical characteristics, organic–inorganic halide perovskites have acquired considerable attention among different technologies, resulting in better performance in optoelectronic and photovoltaic devices [2,3]. Since, 2009 Perovskite materials were employed as a solar cell absorber [1]. The general structure of these materials is *ABX3*, where *A* denotes the organic methylammonium (CH3NH3 +) ion [4] or formamidinium (NH═CHNH3+) ion [5,6] *B* denotes the inorganic cation Pb2$^+$, Sn2+, and *X* can be a halogen ion, I$^-$, Br$^-$, or Cl$^-$. The perovskites materials are an intriguing option for solar cell applications, primarily linked to its remarkable optical and electrical performance, in terms of direct band gap, panchromatic light absorption, high carrier mobility, exciton binding energy in the range of 2 meV and long diffusion length [7]. In addition, the possible controllability of perovskite film quality makes it advantageous when compared with other materials, this fact is ensured by several methods which can minimize the defect density leading to an improved performance [8,9]. The approved power conversion efficiency (PCE) of 25.2% was achieved due to these specific characteristics [10]. A conventional structure was built using penetrated perovskite materials (absorber region) into the mesoporous metal oxide sheet (electrons transport material ETM) and capped at the top by another layer (holes transport material HTM) [11].

TiO_2 as ETM is one of the best efficiency result recorded to date in perovskite based solar cells (PSCs) to our knowledge. Nevertheless, an elevated temperature annealing (500 °C) is mandatory to obtain the crystalline rutile phase that prevents the use of PSCs (Perovskite based solar cells) in flexible devices [12]. Also, TiO_2 shows instability in the UV range and provides a low value of electron mobility [13]. Researchers employed a decreased temperature solution-processed ZnO as ETM to prevent such drawbacks and they estimated a PCE of 15.7% in

* Corresponding author. Faculty of Technology, University of M'sila, 28000, Algeria.
E-mail addresses: toufik.bendib@univ-msila.dz, toufikdzdz@gmail.com (T. Bendib).

https://doi.org/10.1016/j.optmat.2020.110259
Received 30 June 2020; Received in revised form 15 July 2020; Accepted 23 July 2020
Available online 18 August 2020

planar PSCs [14]. These findings allowed novel ways to substitute TiO_2 to other ETM in PSCs for high-efficiency. In 2015, researchers reported a PCE of 16.02% when a solution-processed low-temperature SnO_2 material was employed in standard PSC structure with a reduced amount of hysteresis [15]. In another study, SnO_2 was utilized in planar PSCs as an effective ETM synthesized via low temperature ALD process, yielding 18% conversion efficiency with no hysteresis [16]. New outcomes with SnO_2 as an ETM in PSCs demonstrate good efficiency in planar architecture comparable to TiO_2 and ZnO, with V_{oc} of 1090 mV and efficiency of 20.3%, and SnO_2 gained further consideration because of its electronic construction [17].

However, the usage of the organic molecule which is based on Spiro-OMeTAD as HTM affects the proprieties of these promising PSCs. To function as a competent HTM the Spiro-OMeTAD requires dopants and additives similar to hygroscopic LiTFSI salt and t-BP, which is a source of instability for the perovskite solar cells [18]. In addition, perovskite losses which are a significant portion of the overall cost (about 34%) of the device are linked to the HTM and cathode materials [19]. Numerous small organic molecules, semiconductors, polymers and organo-metallic compounds were used as HTM in perovskite based solar cells to substitute Spiro-OMeTAD, and showed considerable PV results [20]. Although, only some of these materials were found to present some advantages in terms of atmospheric stability, additional enhancements are required for high performance perovskite applications including the ETM/HTM quality aspect. Although, a significant work has been carried out and many papers were published and exist in literature, related to the performance and improvement of PSCs [21–25], but only few studies were focused on both optical and electrical modeling of these devices which remains crucial and complementary to their electrical characterization [26–29]. Moreover, the analysis of the appropriate ETM and HTM materials that takes into account device fabrication and experimental work like testing procedure is found very expensive and time consuming.

Hence, in order to address these issues which hinder the commercialization of perovskite based solar cells, numerous materials have been proposed and examined to find the adequate electron and hole transport layers (ETL and HTL) using 1D-SCAPS software simulator. Zinc sulfide (ZnS), Zinc selenide (ZnSe), tin dioxide (SnO_2), titanium dioxide (TiO_2) and zinc oxide (ZnO), ITO are suggested as an ETM. The investigated HTM materials are: Spiro-OMeTAD [(2,2′,7,7′-tetrakis-(N,Ndi-*p*-methoxyphenyl-amine)-9,9′-spirobifluorene)], Cu2O and Nickel (II) oxide NiO, P3HT and PEDOT:PSS. 1D-SCAPS simulator resolves under steady state conditions the 1D equation which manages the semiconductor material. Nevertheless, the disadvantages, we have encountered with SCAPS, are the inappropriate account of the reflection at different interfaces and the inaccurate calculation of the absorption and generation rate causing an underestimation of the solar cells performance.

To account for the latter, a combined optical-electrical approach based on the TMM and Scaps 1D simulator is proposed to model the investigated n-i-p PSC. Many researchers have performed a theoretical analysis on the optical and electrical performance of perovskite solar cells employing transfer-matrix approach [30] or finite difference time domain method [31]. A three dimensional (3D) COMSOL simulator utilizing the finite element method (FEM) is also suggested [32]. The aforementioned methods prove their effectiveness in modeling perovskite solar cell performance accurately when dealing with complex structures including light trapping formalisms and surface plasmonics designs [32,33]. However, these tools are time consuming. So, for simple planar device, Scaps 1d simulator is an intriguing option for reducing the computation time. By coupling this simulator with transfer matrix method we will also ensure the calculation accuracy of the device optical characteristics. The proposed optical-electrical approach serves mainly for the investigation of appropriates ETM and HTM candidates that meet the design requirement in terms of good band alignment and suitable optical characteristics. Also this approach is suitable for reducing the time consuming when compared with other powerful tools for simple planar structures. The obtained results indicate clearly that our optimized PSC design using ZnO as ETM and NiO as HTM surpasses considerably the PSC using other ETM and HTM candidates. The proposed approach leads to better understanding both optical and electrical proprieties of these structures and highlights their high quality in terms of solar cells performance. This result makes the proposed approach an intriguing option for solar cells optimization.

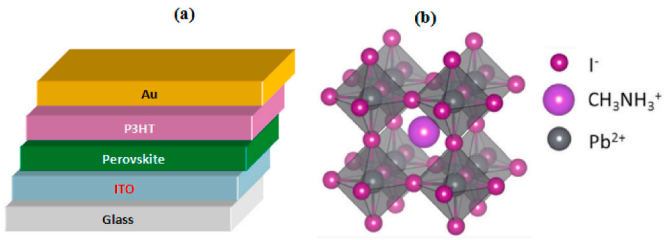

Fig. 1. (a) Conventional structure of perovskite based solar cell (b) Perovskite CH3NH3PbI3 crystal structure [34].

Table 1
Input data of baseline ITO/CH3NH3PbI3/P3HT structure.

Parameters	Unit	ETL (ITO)	Perovskite	HTL (P3HT)
Thickness	nm	5	400	5
Eg	eV	3.65	1.55	1.58
X	eV	4.8	3.9	3.1
ε_r	/	8.9	6.5	3.4
N_c	cm^{-3}	2.2×10^{18}	2.2×10^{18}	1×10^{22}
N_v	cm^{-3}	1.9×10^{19}	1.9×10^{19}	1×10^{22}
μ_n	$cm^2\ v^{-1}s^{-1}$	10	2	10^{-4}
μ_p	$cm^2\ v^{-1}s^{-1}$	10	2	10^{-3}
N_d	cm^{-3}	1×10^{20}	2×10^{13}	/
N_a	cm^{-3}		/	1×10^{16}
N_t	cm^{-3}	1×10^{15}	2.5×10^{13}	1×10^{14}

2. Device structure and transport mechanism

Fig. 1 presents the investigated perovskite (CH3NH3PbI3) based solar cell considering n-i-p structure.

From top to bottom it consists of a metal contact (Au), an HTL material type p (P3HT), an intrinsic perovskite material which functions as an absorber and n type ETL material (ITO). The perovskite (*region i*) is a site of exitons creation (electron and a hole bound state) when the solar cell are illuminated. The photogenerated carriers (electrons and holes) are collected in ETL and HTL regions. The collection mechanism of electrons (holes) is related to their diffusion length and ETL (HTL) electrical properties. The separation of exitons occurs at the interfaces ETL/perovskite and perovskite/HTL. The electrons migrate to the ETL region (n) and the holes move to the HTL region (p). The dissociation and migration mechanisms are caused by the electric field between the ETL and HTL. The input data of the conventional perovskite based solar cell ITO/perovskite/P3HT are recapitulated in Table 1.

We perform the simulation considering AM1.5 G solar spectrum. Where, the input parameters of perovskites data are taken from literature [25,30,34].

3. Materials and methods

In this work, by using the transfer matrix method (TMM), the reflection, transmission, and absorption coefficient are calculated. Besides, the refractive indices' imaginary and real parts of each ETM and HTM materials are extracted from the literature, sulfide (ZnS) [35], Zinc selenide (ZnSe) [36], tin dioxide (SnO_2) [37], titanium dioxide (TiO_2) [38] and zinc oxide (ZnO) [39], indium-tin-oxide (ITO) [40], Cu_2O [41]

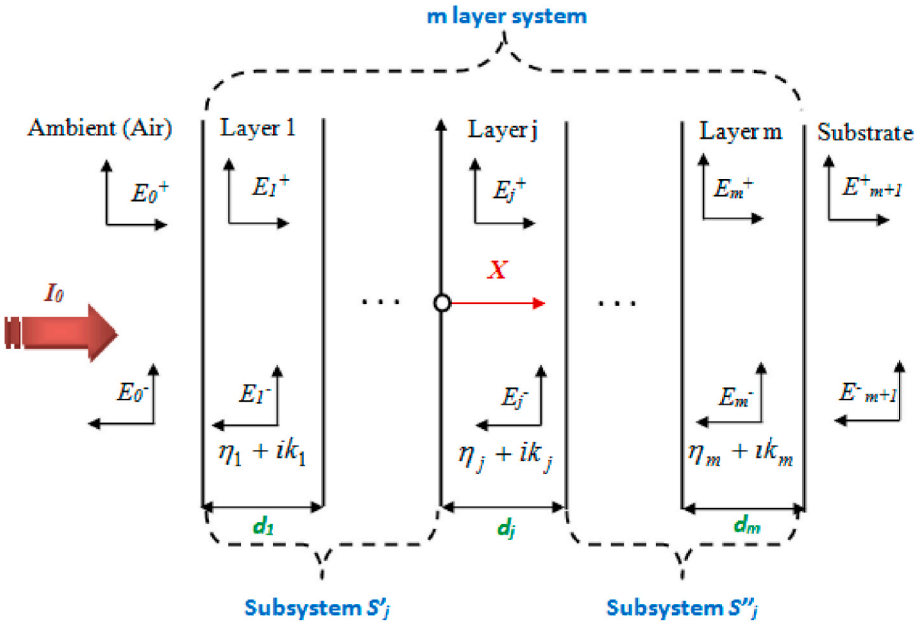

Fig. 2. Representation of the investigated structure sandwiched between ambient and substrate [45].

and NiO [37], Spiro-OMeTAD [42], P3HT [43] and PEDOT:PSS [44].

3.1. Optical modeling

The TMM was employed to predict the main outputs of PSCs [38]. TMM assumes a normal incidence of the incoming light through a thin film device. Fig. 2 illustrates the incidence of the plane wave from layer 1 to layer m, sandwiched between transparent ambient and substrate. Owing to the interference outcome inside the structure at any point x in layer j, the resulting optical electric field is constituted from a positive part $E_j^+(x)$ and a negative part $E_j^-(x)$. The use of the complex refraction index of $\tilde{n}_j = n_j + ik_j$ and thickness d_j is essential to describe the optical properties of each j layer.

The optical transfer matrices are described by the interface matrix which describes each interface I_{jk} and the layer matrix that define the propagation through layer j.

The light activity at the $j/k = j + 1$ layers of the interface can be described by a 2 × 2 matrix that includes the complex coefficients of Fresnel.

The interface matrix I_{jk} is expressed as follows:

$$I_{jk} = \begin{bmatrix} (\tilde{n}_j + \tilde{n}_k)/2\tilde{n}_j & (\tilde{n}_j - \tilde{n}_k)/2\tilde{n}_j \\ (\tilde{n}_j + \tilde{n}_k)/2\tilde{n}_j & (\tilde{n}_j + \tilde{n}_k)/2\tilde{n}_j \end{bmatrix} \quad (1)$$

The layer matrix L_j is given as follows:

$$L_j = \begin{bmatrix} \exp\left(-i\frac{2\pi\tilde{n}_j}{\lambda}d_j\right) & 0 \\ 0 & \exp\left(-i\frac{2\pi\tilde{n}_j}{\lambda}d_j\right) \end{bmatrix} = \begin{bmatrix} \exp(-ik_j d_j) & 0 \\ 0 & \exp(-ik_j d_j) \end{bmatrix} \quad (2)$$

where, $k_j = 2\pi n/\lambda$ and d_j represent the monolayer thickness. The phase propagation is described by the real part of the complex refraction index $\tilde{n}_j$ and the light absorption is described by the imaginary part k.

The total transfer matrix is estimated by multiplying all the calculated transfer matrices in the devices. It associates the optical electric field of the 0^{th} monolayer and the $(m+1)^{th}$ monolayer and it can be expressed as,

$$\begin{bmatrix} E_0^+ \\ E_0^- \end{bmatrix} = S \begin{bmatrix} E_{m+1}^+ \\ E_{m+1}^- \end{bmatrix} \quad (3)$$

The total transfer matrix S is expressed as follows:

$$S = \begin{bmatrix} S_{11} & S_{12} \\ S_{21} & S_{22} \end{bmatrix} = \left(\prod_{v=1}^{m} I_{(v-1)v} L_v\right) I_{m(m+1)} \quad (4)$$

The general equation that describes the optical electric field distribution in the device at each layer j is expressed as follows:

$$E_j(x) = E_j^+(x) + E_j^-(x) \quad (5)$$

where $E_j^+(x)$ and $E_j^-(x)$ are calculated by solving iteratively the matrix equation (3) using the transfer matrix of equation (4).

After some mathematical manipulation, the total optical electric field is given as follows:

$$E_j(x) = E_j^+(x) + E_j^-(x) = t_j^+ \left[e^{ik_j x} + r_j'' e^{ik_j(2d_j - x)}\right] E_0 \quad (6)$$

where, E_0 represents the incident light's electric field from the ambient, t_j^+ and r_j'' are the complex transmission and reflection coefficients calculated at each layer j in the device.

$$t_j^+ = \left[S_{j11}' + S_{j12}' r_j'' e^{2ik_j d_j}\right]^{-1} \quad (7)$$

$$r_j'' = S_{j21}'' / S_{j11}'' \quad (8)$$

S_j' and S_j'' are partial transfer matrices subtracted from the transfer matrix S in equation (4)

$$S_j' = \begin{bmatrix} S_{j11}' & S_{j12}' \\ S_{j21}' & S_{j22}' \end{bmatrix} = \left(\prod_{v=1}^{j-1} I_{(v-1)v} L_v\right) I_{(j-1)j} \quad (9)$$

$$S_j'' = \begin{bmatrix} S_{j11}'' & S_{j12}'' \\ S_{j21}'' & S_{j22}'' \end{bmatrix} = \left(\prod_{v=j+1}^{m} I_{(v-1)v} L_v\right) I_{m(m+1)} \quad (10)$$

The incoming beam of light intensity flowing a particular layer j in the device can be defined as:

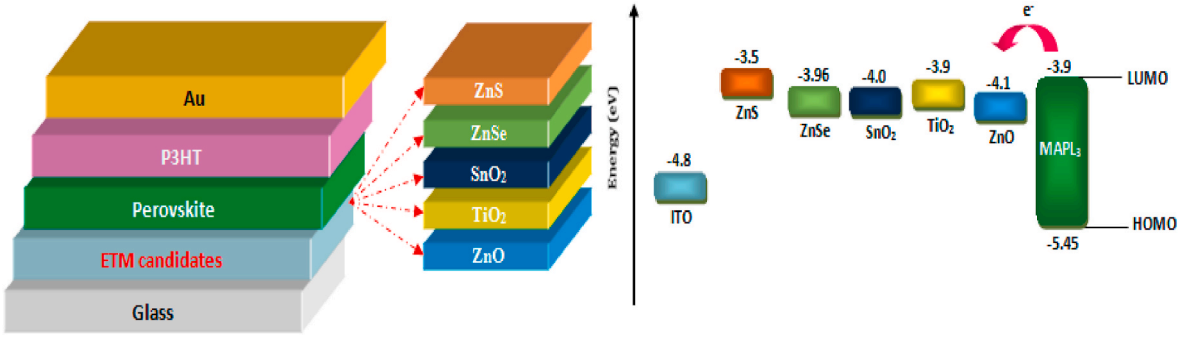

Fig. 3. Schematic of the device structure and energy band diagram alignment between perovskite and different ETM candidates.

$$I_j(x,\lambda) = T_j I_0(\lambda)\left[\begin{array}{l} e^{-\alpha_j x} + \rho_j^{''2}\, e^{-\alpha\left(2d_j - x\right)} \\ +2\rho_j^{''} e^{-\alpha_j d_j}\cos\left(\dfrac{4\pi n_j}{\lambda}\left(d_j - x\right) + \delta_j^{''}\right) \end{array}\right] \tag{11}$$

where $I_0(\lambda)$ denotes the intensity of the incident light, $T_j=(n_j n_0)t_j^2$ represents the internal intensity transmittance, $\rho_j^{''}$ and $\delta_j^{''}$ refers to the reflection coefficient's absolute and argument components. The dissipation of energy Q can be calculated as:

$$Q(x,\lambda) = \alpha\,(\lambda)\, I\,(x,\lambda) \tag{12}$$

The active layer's exciton generation rate is calculated using the following formula:

$$n\ (x) = \int \frac{\lambda}{hc} Q\,(x,\lambda)\, d\lambda \tag{13}$$

where h and c represent the plank constant and speed of light in vacuum, respectively.

The total complex reflection and transmission coefficients of the whole stacked layers system can be expressed as follows:

$$r = \frac{E_0^-}{E_0^+} = \frac{S_{21}}{S_{11}} \tag{14}$$

$$t = \frac{E_{m+1}^+}{E_0^+} = \frac{1}{S_{11}} \tag{15}$$

The transmittance and reflectance of the investigated system are calculated using the following expression:

$$R = |r|^2 \tag{16}$$

$$T = |t|^2 \frac{\eta_{m+1}}{\eta_0} \tag{17}$$

The absorption coefficient is calculated using the following formula:

$$\alpha = \frac{4\pi k}{\lambda} \tag{18}$$

3.2. Electrical modeling

SCAPS-1D software is an actualized 1D solar cell tool suitable to simulate numerically different solar cells structures [46]. SCAPS-1D solves numerically 1D semiconductor equations under steady-state conditions. A combined Gummel and Newton– Raphson methods are used for convergence. On the other side, we assume a drift–diffusion model to define the transport of photo-generated carriers. Poisson equations with interfaces and contacts boundary conditions are usually expressed as follows:

$$\frac{\partial}{\partial x}\left(\varepsilon_0 \varepsilon_r \frac{\partial}{\partial x}\phi(x)\right) = q\left(p(x) - n\,(x) + N_D^+ - N_A^- \rho_{def}\right) \tag{19}$$

Table 2
Input SCAPS parameters of ETMs.

Parameters	Unit	SnO_2	TiO_2	ZnO	ZnSe	ZnS
Eg	eV	3.5	3	3.3	2.81	3.6
χ	eV	4	4	4.1	4.09	4.45
ε_r	/	9	9	9	8.6	9
N_c	cm^{-3}	2.2×10^{18}	2.2×10^{18}	2.2×10^{18}	2.2×10^{18}	2.2×10^{18}
N_v	cm^{-3}	1.9×10^{19}	1.9×10^{19}	1.9×10^{19}	1.9×10^{19}	1.9×10^{19}
μ_n	$cm^2 v^{-1}s^{-1}$	20	20	100	400	100
μ_p	$cm^2 v^{-1}s^{-1}$	10	10	25	110	25
N_d	cm^{-3}	1×10^{18}	1×10^{18}	1×10^{18}	1×10^{18}	1×10^{18}
N_t	cm^{-3}	1×10^{15}	1×10^{15}	1×10^{15}	1×10^{15}	1×10^{18}

$$-\frac{\partial}{\partial x}J_p(x) + G(x) - R(x) = \frac{\partial p}{\partial t} \tag{20}$$

$$-\frac{\partial}{\partial x}J_n(x) + G(x) - R(x) = \frac{\partial n}{\partial t} \tag{21}$$

$$J_p = \frac{\mu_p}{q} p \frac{\partial E_{Fp}}{\partial x} \tag{22}$$

$$J_n = -\frac{\mu_n}{q} n \frac{\partial E_{Fn}}{\partial x} \tag{23}$$

where, $\phi(x)$ represents the electrostatic potential, ε_0, ε_r refers to the dielectric constant of both vacuum and perovskite material, respectively. $n(p)$ denotes the concentration of released electrons (holes), N_D (N_A) represent the ionized donors (acceptors) density. ρ_{def} represents the defects charge density, R and G denotes the recombination and generation rates, respectively. J_n (J_p) represent the electron (hole) current density. $E_{Fn(p)}$ is quasi-Fermi level for electrons (holes). μ_n (μ_p) is the electron (hole) mobility.

4. Results and discussions

4.1. Effect of the electron transport material

In this section, we propose a number of ETMs for investigation to achieve high performance PSCs. The schematic diagram of the device structure with different ETM candidates and their bands alignment are depicted in Fig. 3. We assume a thickness of 0.05 μm for ETM candidates, where the perovskite based solar cell structures using as ETM: Zinc sulfide (ZnS), Zinc selenide (ZnSe), tin dioxide (SnO_2), titanium dioxide (TiO_2) and zinc oxide (ZnO) are examined against the conventional structure that use ITO as ETM.

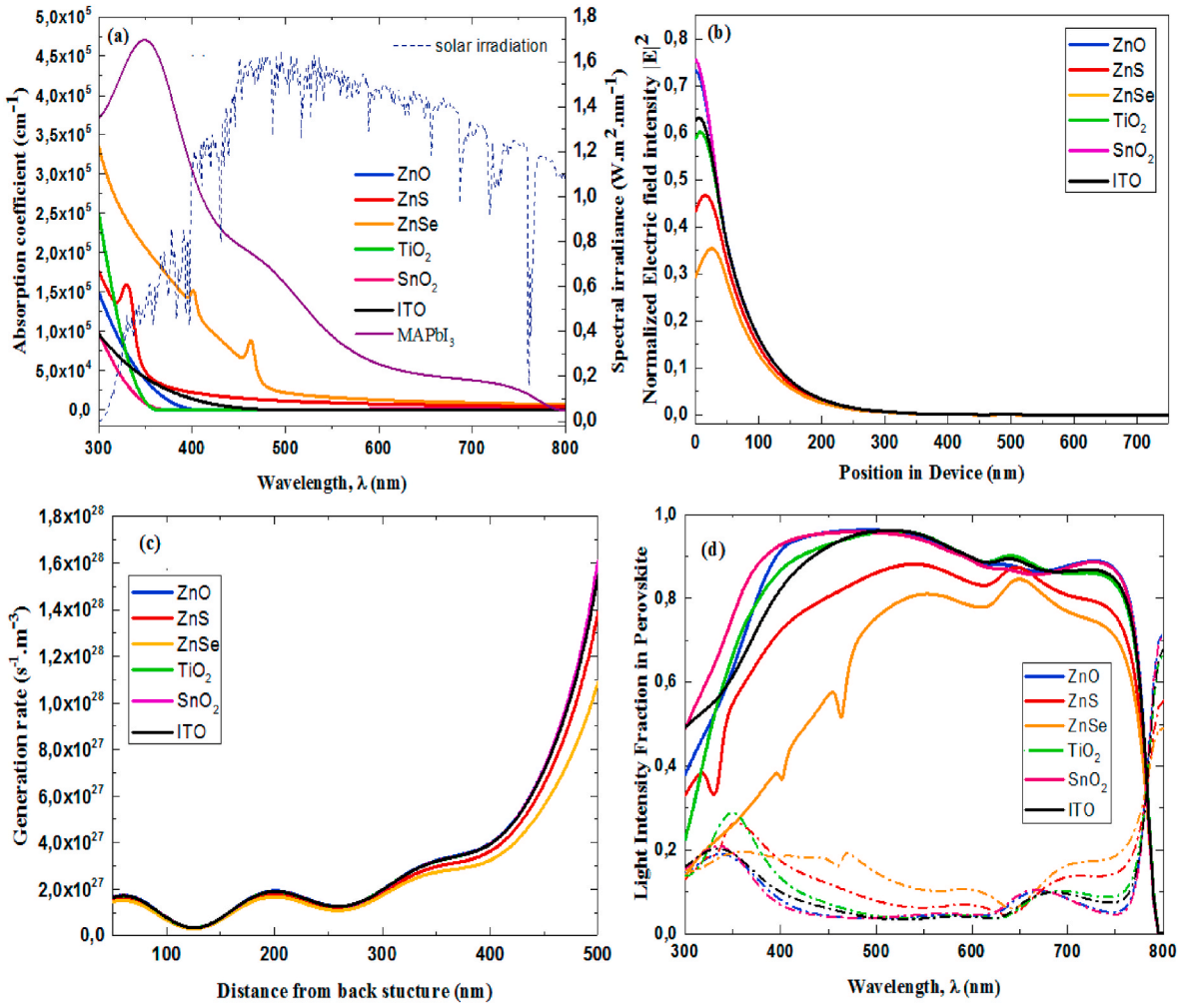

Fig. 4. Optical properties of ETM candidates **(a)** Absorption coefficients Vs wavelength of ETMs/PVK **(b)** Electric field intensity in the device **(c)** Generation rate in perovskite layer for P3HT/PVK/different ETM structures **(d)** Light intensity fraction in perovskite based solar cell, absorbed (solid line) reflected (dashed line).

The main parameters of the investigated ETM are recapitulated in Table 2. It is noticeable that input data of SnO_2, TiO_2, ZnO, ZnSe and ZnS are extracted from literature [22–26].

A key element to choose the appropriate ETM material is by establishing a careful balance between electrical conductivity and optical transmittance. Enhancing the electrical conductivity include a possible rise in carrier mobility, which leads however to an increase in the visible absorption. In this context, we investigate a suitable ETM candidate which overcomes this tradeoff. Interference fringes in the visible spectrum are displayed. These are obtained from reflectance and/or

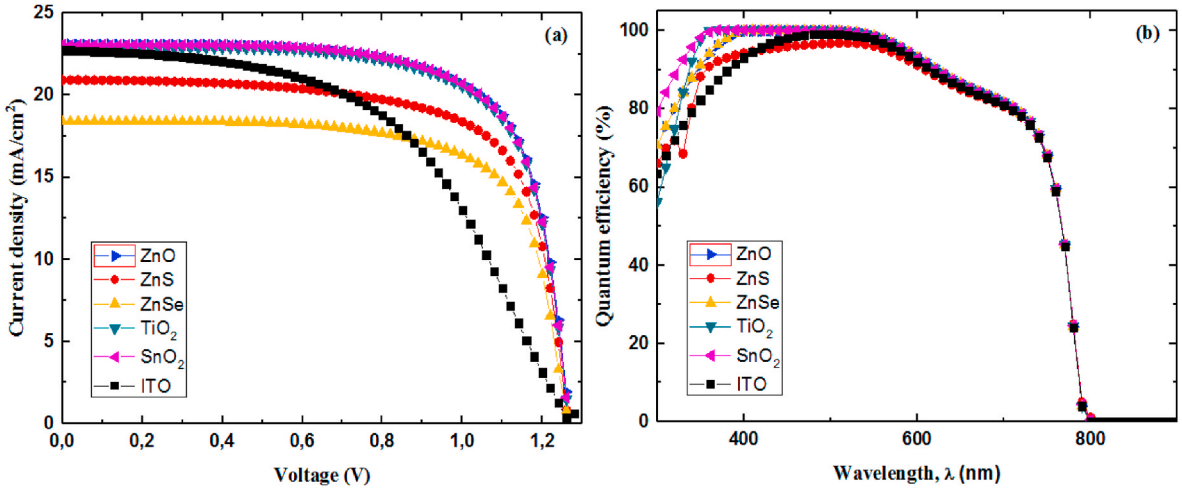

Fig. 5. Influence of different ETM candidates on the CH3NH3PbI3 based solar cell performance using P3HT as HTM (a) *J-V* characteristics (b) Quantum efficiency.

Table 3
The investigated perovskite solar cells figures of merit with different ETM candidates.

Parameters	ITO	SnO_2	TiO_2	ZnO	ZnSe	ZnS
V_{oc} (V)	1.268	1.266	1266	1.268	1.256	1.263
J_{sc} (mA/cm^2)	22.728	23.061	22,88	23.083	18.409	20.928
FF (%)	52.52	71.52	71,49	71.57	71.24	70.28
η (%)	15.13	20.88	20,71	20.95	16.47	18.58
V_{MPP} (V)	0.840	1.040	1,04	1.060	1.040	1.060
J_{MPP} (mA/cm^2)	18.016	20.086	19,912	19.760	15.843	17.533

transmittance of ETM films. Even though, the transmittance shows a high value exceeding 85%, this may appear to be not a practical average across the operational spectrum. Alternatively, we use the absorption coefficient to accurately assess the ETM candidates. Fig. 4-a shows the absorption coefficients spectra as function of optical wavelength.

From Fig. 4-a it is clearly shown that ZnSe and ZnS have an overlap of the absorption in the visible range which cause a solar cell performance degradation. In comparison, ZnO, SnO_2 and TiO_2 show a high transparence in the visible range.

The electrical field at the interfaces ETM/perovskite and perovskite/HTM is responsible for exitons dissociation and electrons (holes) migration. It is worth noticing that the rate of exciton dissociation increases with increasing electric field. Fig. 4-b represents the variation of the normalized electric field intensity along distance. It is obvious from this figure that PSC using ZnO or SnO_2 as ETM exhibits a high electric field. This fact will enhance the separation mechanism leading to the increase of the conversion efficiency.

The generation rate of perovskite based solar cell is plotted in Fig. 4-c. It is obvious from this figure that a PSC using ZnO and SnO_2 as ETL layer exhibits high generation rate, this fact is linked to the low visible spectrum absorption and the improved electric field. It is also worth to notice that after the optical modeling characterization, TiO_2 shows a less optical performance compared to ZnO and SnO_2 counterpart. This might be clarified by the fact that a system can difficultly function as a photonic crystal when there is a slight difference in the refractive index between ETM and perovskite materials [47]. Comparable refractive index values of TiO_2 and Perovskite materials, in the range of 500–700 nm, are recognized [48] which hinders the solar cell performance in terms of exciton generation.

The fraction of absorbed and reflected Light in Perovskite for different ETM candidates (P3HT/PSK/ETL) is shown in Fig. 4-d. As mentioned previously, PSC using ZnO and SnO_2 shows a good performance in terms of absorption, this mainly attributed to the suitable gap and refractive index. In contrast, ZnSe and ZnS exhibit a low absorption fraction.

Fig. 5-a shows the *J-V* characteristics where the extracted output parameters are recapitulated in Table 3. From this figure, it is clearly observed that ITO displays low current density *Jsc* of 22.728 mA/cm^2 compared to the other materials as well as an inferior value of quantum efficiency (QE) is remarked in Fig. 5-b. The reduced outcome can be attributed to the reduced electron and holes mobilities (10 cm^2/Vs), which influence the collection of charges. In contrast, the tin dioxide (TiO_2) exhibits the maximum yields in terms of open circuit voltage and fill factor (*Voc* = 1.266*V*, *FF* = 71.49%), which allow to reaching a power conversion efficiency of 20.71%. (SnO_2) and (ZnO) showed an improved *QE* and analogous high efficiency values (20.88% and 20.95%, respectively). These materials display approximately similar figures of merit values (*Voc* = 1.27 *V*, *Jsc* = 23.08 mA/cm^2, *FF* = 71.5% and η = 20.9%.). Fig. 3 shows different ETMs band alignment with perovskite absorber. From this figure a slight dissimilarity in the band energy between ZnO, TiO_2 and SnO_2 and perovskite material is observed (Similar affinity and energy gap, ZnO have high carrier mobility).

Table 4
Input SCAPS parameters of HTM materials.

Parameters	Unit	PEDOT: PSS	Cu_2O	NiO	Spiro_Ometad
Eg	eV	2.2	2.1	3.6	3
X	eV	2.9	3.2	1.8	2.45
ε_r	–	3	7.11	11.75	3
N_c	cm^{-3}	1×10^{21}	2.2×10^{18}	2.2×10^{18}	2.2×10^{18}
N_v	cm^{-3}	1×10^{21}	1.9×10^{19}	1.9×10^{19}	1.9×10^{19}
μ_n	cm^2 v^{-1}s^{-1}	2×10^{-2}	3.4	2×10^{-1}	2×10^{-4}
μ_p	cm^2 v^{-1}s^{-1}	2×10^{-4}	3.4	2×10^{-1}	2×10^{-4}
N_a	cm^{-3}	1×10^{18}	1×10^{18}	1×10^{18}	1×10^{18}
N_t	cm^{-3}	1×10^{15}	1×10^{15}	1×10^{15}	1×10^{15}

The best efficiency conversion recorded for tin dioxide (ZnO) which seems to be an intriguing choice as ETM with conversion efficiency up to 20.95%. This may be attributed to the appropriate band alignment of ZnO's conduction band with the LUMO of the perovskite material. Also the outstanding properties of this material such as high transparence, high carrier mobility and suitable refractive index all of make it at the top of ETL materials. The results in Table 3 are estimated for P3HT/Perovskite/different ETL materials.

4.2. Effect of the hole transport material

In the following, we focus on ZnO as the main ETM candidate because the results of the other candidates are not available. In the same way as previously, we investigate in this section different organic and inorganic materials as HTM. The schematic diagram of the device structure with different HTM candidates and their bands alignment are plotted in Fig. 6.

The proposed HTMs are: Spiro-OMeTAD (2,2′,7,7′-tetrakis-(N,Ndi-*p*-methoxyphenyl-amine)-9,9′-spirobifluorene)], Cu2O and Nickel (II) oxide NiO, P3HT and PEDOT:PSS. Data for these materials are taken from literature [22–25,30]. The input parameters are presented in Table 4.

An HTM mainly performs two important tasks namely, accelerate the transport of the photogenerated holes to the counter electrode; and avoid the direct interaction amid the electrode and the active layer. The aforementioned tasks are critical in achieving high efficiency and stability. The absorption of HTM is always ignored but reflection is

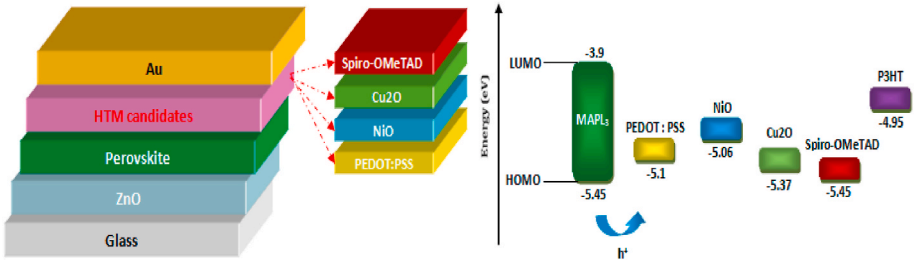

Fig. 6. Schematic of the device structure and energy band diagram alignment between perovskite and different HTM candidates.

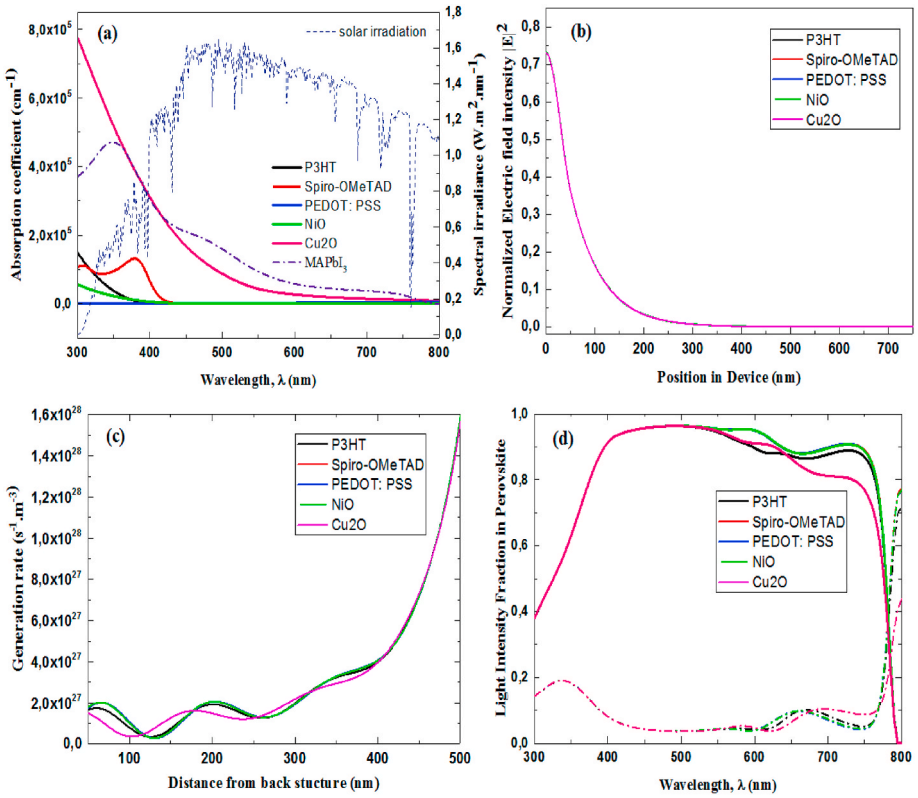

Fig. 7. Optical properties of HTM candidates **(a)** Absorption coefficients Vs wavelength of HTMs/PVK **(b)** Electric field intensity in the device **(c)** Generation rate in perovskite layer for P3HT/PVK/different ETM structures **(d)** Light intensity fraction in perovskite based solar cell, absorbed (solid line) reflected (dashed line).

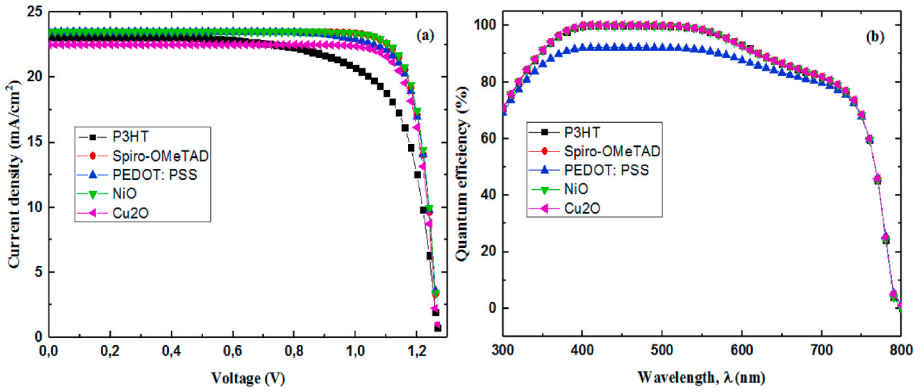

Fig. 8. Fig. 5: Influence of different HTM candidates on the CH3NH3PbI3 based solar cell performance using ZnO as ETM (a) *J-V* characteristics (b) Quantum efficiency.

considered to contribute to the generation of carriers. In order to investigate the effect of the optical properties of HTM candidates on the solar cell performance, a TMM method is adopted and the calculated properties are inserted into Scaps 1D simulator. Fig. 7 displays the optical performance of the investigated solar cell with different HTMs.

Fig. 7-a shows the variation of absorption coefficient as function of wavelength. It can be seen form this figure that all material except Cu2O are transparent in the visible range. However, Fig. 7-b and d show that the absorption do not affect the performance of the PSC. Fig. 7-c represents the generation rate in the device as function of distance from back structure for different HTMs. From this figure, it is shown that using a material like NiO, PEDOT: PSS, Spiro-OMeTAD may enhance the device generation rate, this fact could be to relate the adequate refractive index of this materials which makes light to interfere at the back of the cell destructively.

By assuming a ZnO ETL thickness of 0.05 μm, different HTM candidates will be examined. Fig. 8 shows the *J-V* characteristic and the quantum efficiency, respectively. From this graph it can be seen that the absorption of HTMs candidates do not influence the solar cell performance. This fact is mainly due to the location of this material at rear side of the device. Another finding, concerns the *J-V* curve is the remarkable enhancement of the PSC performance in terms of short circuit current and fill factor. This fact is attributed to the suitable bands alignment between the HOMO of perovskite material and valence band of HTM candidates (Fig. 9). However a reduced short circuit current is noticed for Cu2O. Decreased conversion efficiency is observed for a solar cell using P3HT as HTM, this fact is due mainly to the high difference between the HOMO levels of MAPbI3 and P3HT which is around 0.5 eV.

On the other hand, an improved efficiency is achieved using NiO (24.94%) with a fill factor equal to 83.77% as recapitulated in Table 5.

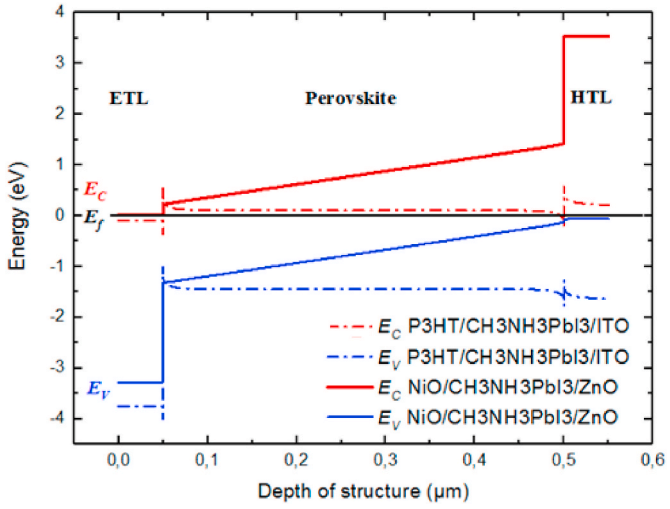

Fig. 9. Comparison of Energy Band diagram between the optimized perovskite based solar cell and the conventional one.

Table 5
The investigated perovskite solar cells figures of merit with different HTM candidates.

Parameters	P3HT	PEDOT:PSS	Cu2O	NiO	Spiro_Ometad
V_{oc} (V)	1268	1269	1265	1268	1268
J_{sc} (mA/cm^2)	23,083	23,488	22,511	23,487	23,497
FF (%)	71,57	81,50	83,40	83,7714	83,53
η (%)	20,95	24,290	23,75	24,94	24,89
V_{MPP} (V)	1.060	1,12	1,1	1,12	1,1
J_{MPP} (mA/cm^2)	19.760	21,687	21,596	22,271	22,631

The obtained figures of merit values when using ZnO as ETL and NiO as HTL are: $Voc = 1.268$ *V*, $Jsc = 23.48$ mA/cm^2, $FF = 83.77\%$ and $\eta = 24.94\%$. These findings prove the advantage of the optimized structure against the conventional configuration using ITO as ETL and P3HT as HTL, where an improvement of about 9.81% in power conversion efficiency and about of 31.25% in *FF* is reached.

Table 6
Figures of merit for different structures taken from literature.

PVK structure	J_{SC} (mA/cm^2)	V_{OC} (V)	*FF* (%)	η (%)	*Reference*
TiO2/FASnI 3/Spiro-MeOTAD	22.65	0.92	67.74	14.03	[21]
FTO/SnO_2/MAPbI3/CuSCN/Au	25.61	1.19	87.81	26.74	[22]
CuSCN/CH3NH3PbI3/TiO_2	24.70	1.23	82.5	25.02	[23]
CuSbS2/CH3NH3GeI3/ITO	23.59	1.66	60.29	23.58	[24]
CuSCN/CH3NH3PbI3/TiO_2	24.29	1.00	62.7	15.23	[26]
Ag/CuSCN/CH3NH3PbI3/TiO_2	23.53	1.011	65.4	15.38	[27]
Au/CuSCN/CH3NH3PbI3/TiO_2	22.13	/	/	14.89	[33]
NiO/CH3NH3PbI3/ZnO	23.84	1.268 V	83.77	24.94	This work

This improvement is attributed to the compromise made between high hole mobility and good band alignment. Solar cell using Spiro- OMeTAD shows comparable conversion efficiency as NiO. It is noticeable that Spiro- OMeTAD has the best band alignment but exhibits a low hole mobility in comparison with NiO.

Fig. 9 depicts the comparison of energy band diagram between the optimized perovskite based solar cell and the conventional one. As shown in Fig. 9, a suitable band alignment between the NiO's valence band and the HOMO of perovskite absorber is achieved. Furthermore, ZnO 's energy bands fulfill the key criteria for high-performance PSCs: Its conduction band (CB) is situated below the perovskite layer CB to tear off electrons entering the interfaces. (2) ZnO layer rejects the holes because its valence band (VB) lies well beneath the perovskite's VB. (3) Owing to a large difference in terms of BV between ZnO and perovskite, ZnO ETM can efficiently reject holes. Another finding that can enlighten the suitability of ZnO as ETM is their high electron mobility and suitable refractive index (not close to perovskite index) leading to high absorption coefficient. Besides, NiO accelerate the transport of the photo-generated holes to the counter electrode; and avoid the direct interaction amid the electrode and the active layer.

Finally, Table 6 reports the state of the art in term of figures of merit (J_{SC}, V_{OC}, *FF* and efficiency) for different perovskite solar cell structures taken from literature [21–33].

We can conclude that the optimized perovskite solar cell exhibits a good performance compared to other devices. In addition, investigating an optimized light trapping morphology will further improve the device in terms of short circuit current [26,27], which pave the way in the future to reach high performance and boost up the device conversion efficiency.

5. Conclusion

The purpose of this work was the investigation of an optimized design of n-i-p perovskite based solar cell by means of combined optical and electrical approach. Transport proprieties of the charge carrier electron (hole) are studied in order to determine the role of the main factors which improve the efficiency of the solar cell. An optimized structure with Zinc oxide (ZnO) as ETM and Nickel(II) oxide (NiO) as HTM outperforms the conventional solar cell. The proposed ETM and HTM materials satisfy the requirement in terms of high optical performance and good band alignment which enhances the solar cell electrical efficiency. Although, the proposed approach has proven to be reliable for a particular perovskite based solar cell, it is in principle appropriate for different tandem solar cells. The proposed coupled model can be extended by using intelligent artificial methods for global optimization in order to obtain the optimal parameters which affect the efficiency of the solar cells such as thickness and doping concentrations of the absorber layer.

Declaration of competing interest

The authors declare that they have no known competing financial interests or personal relationships that could have appeared to influence the work reported in this paper.

Acknowledgements

This work was supported by DGRSDT of Ministry of Higher education of Algeria.

References

[1] A. Kojima, K. Teshima, Y. Shirai, T. Miyasaka, Organometal halide perovskites as visible-light sensitizers for photovoltaic cells, J. Am. Chem. Soc. 131 (2009) 6050–6051, https://doi.org/10.1021/ja809598r.
[2] W.J. Yin, J.H. Yang, J. Kang, Y. Yan, S.H. Wei, Halide perovskite materials for solar cells: a theoretical review, J. Mater. Chem. 3 (17) (2015) 8926–8942, https://doi.org/10.1039/C4TA05033A.
[3] Z. Wang, P. Li, Z. Liu, J. Fan, X. Qian, J. He, P. Gao, Hole selective materials and device structures of heterojunction solar cells: recent assessment and future trends, Apl. Mater. 7 (11) (2019) 110701, https://doi.org/10.1063/1.5121327.
[4] S. Kazim, M.K. Nazeeruddin, M. Grätzel, S. Ahmad, Perovskite as light harvester: a game changer in photovoltaics, Angew. Chem. Int. Ed. 53 (2014) 2812–2824, https://doi.org/10.1002/anie.201308719.

[5] G.E. Eperon, S.D. Stranks, C. Menelaou, M.B. Johnston, L.M. Herz, H.J. Snaith, Formamidinium lead trihalide: a broadly tunable perovskite for efficient planar heterojunction solar cells, Energy Environ. Sci. 7 (2014) 982–988, https://doi.org/10.1039/C3EE43822H.

[6] M. Salado, S. Kazim, M.K. Nazeeruddin, S. Ahmad, Appraisement of crystal expansion in CH3NH3PbI3 on doping: improved photovoltaic properties, Chem. Sus. Chem. 12 (2019) 2366–2372, https://doi.org/10.1002/cssc.201803043.

[7] Q. Lin, A. Armin, R.C.R. Nagiri, P.L. Burn, P. Meredith, Electro-optics of perovskite solar cells, Nat. Photon. 9 (2015) 106, https://doi.org/10.1038/nphoton.2014.284.

[8] Q. Sun, X. Gong, H. Li, S. Liu, X. Zhao, Y. Shen, M. Wang, Direct formation of I3- ions in organic cation solution for efficient perovskite solar cells, Sol. Energy Mater. Sol. Cells 185 (2018) 111–116, https://doi.org/10.1016/j.solmat.2018.05.017.

[9] M. Wang, Z. Zang, B. Yang, X. Hu, K. Sun, L. Sun, Performance improvement of perovskite solar cells through enhanced hole extraction: the role of iodide concentration gradient, Sol. Energy Mater. Sol. Cells 185 (2018) 117–123, https://doi.org/10.1016/j.solmat.2018.05.025.

[10] NREL, Solar cell efficiency chart. https://www.nrel.gov/pv/assets/pdfs/pvefficiencies- 08-02-2019, 2019.

[11] T. Ibn-Mohammed, S.C.L. Koha, I.M. Reaneyc, A.G. Acquayed, K.B. Mustapha, R. Greenough, Perovskite solar cells: an integrated hybrid lifecycle assessment and review in comparison with other photovoltaic technologies, Renew. Sustain. Energy Rev. 80 (2017) 1321–1344, https://doi.org/10.1016/j.rser.2017.05.095.

[12] J. Burschka, N. Pellet, S.-J. Moon, R. Humphry-Baker, P. Gao, M.K. Nazeeruddin, M. Grätzel, Sequential deposition as a route to high-performance perovskitesensitized solar cells, Nature 499 (2013) 316, https://doi.org/10.1038/nature12340.

[13] T. Leijtens, G.E. Eperon, S. Pathak, A. Abate, M.M. Lee, H.J. Snaith, Overcoming ultraviolet light instability of sensitized TiO2 with meso-superstructured organometal tri-halide perovskite solar cells, Nat. Commun. 4 (2013) 2885, https://doi.org/10.1038/ncomms3885, 2013.

[14] D. Liu, T.L. Kelly, Perovskite solar cells with a planar heterojunction structure prepared using room-temperature solution processing techniques, Nat. Photon. 8 (2014) 133, https://doi.org/10.1002/adfm.201302090.

[15] W. Ke, G. Fang, Q. Liu, L. Xiong, P. Qin, H. Tao, J. Wang, H. Lei, B. Li, J. Wan, Low-temperature solution-processed tin oxide as an alternative electron transporting layer for efficient perovskite solar cells, J. Am. Chem. Soc. 137 (2015) 6730–6733, https://doi.org/10.1021/jacs.5b01994.

[16] J.P.C. Baena, L. Steier, W. Tress, M. Saliba, S. Neutzner, T. Matsui, F. Giordano, T. J. Jacobsson, A.R.S. Kandada, S.M. Zakeeruddin, Highly efficient planar perovskite solar cells through band alignment engineering, Energy Environ. Sci. 8 (2015) 2928–2934, https://doi.org/10.1039/C5EE02608C.

[17] E.H. Anaraki, A. Kermanpur, L. Steier, K. Domanski, T. Matsui, W. Tress, M. Saliba, A. Abate, M. Grätzel, A. Hagfeldt, Highly efficient and stable planar perovskite solar cells by solution-processed tin oxide, Energy Environ. Sci. 9 (2016) 3128–3134, https://doi.org/10.1039/C6EE02390H.

[18] Y. Reyna, M. Salado, S. Kazim, A. Pérez-Tomas, S. Ahmad, M. Lira-Cantu, Performance and stability of mixed FAPbI 3(0.85)MAPbBr 3(0.15) halide perovskite solar cells under outdoor conditions and the effect of low light irradiation, Nanomater. Energy 30 (2016) 570–579, https://doi.org/10.1016/j.nanoen.2016.10.053.

[19] J. Gong, S.B. Darling, F. You, Perovskite photovoltaics: life-cycle assessment of energy and environmental impacts, Energy Environ. Sci. 8 (7) (2015) 1953–1968, https://doi.org/10.1039/C5EE00615E.

[20] L. Calió, C. Momblona, L. Gil-Escrig, S. Kazim, M. Sessolo, Á. Sastre-Santos, M. Bolink, M. Grätzel, Inorganic hole conductor-based lead halide perovskite solar cells with 12.4% conversion efficiency, Nat. Commun. 5 (2014) 1–6, https://doi.org/10.1038/ncomms4834, 2014.

[21] S. Abdelaziz, A. Zekry, A. Shaker, M. Abouelatta, Investigating the performance of formamidinium tin-based perovskite solar cell by SCAPS device simulation, Opt. Mater. 101 (2020) 109738, https://doi.org/10.1016/j.optmat.2020.109738.

[22] Y. Raoui, H. Ez-Zahraouy, N. Tahiri, O. El Bounagui, S. Ahmad, S. Kazim, Performance analysis of MAPbI3 based perovskite solar cells employing diverse charge selective contacts: simulation study, Sol. Energy 193 (2019) 948–955, https://doi.org/10.1016/j.solener.2019.10.009.

[23] F. Azri, A. Meftah, N. Sengouga, A. Meftah, Electron and hole transport layers optimization by numerical simulation of a perovskite solar cell, Sol. Energy 181 (2019) 372–378, https://doi.org/10.1016/j.solener.2019.02.017.

[24] A. Hima, N. Lakhdar, Enhancement of efficiency and stability of CH3NH3GeI3 solar cells with CuSbS2, Opt. Mater. 99 (2020) 109607, https://doi.org/10.1016/j.optmat.2019.109607.

[25] S. Bansal, P. Aryal, Evaluation of new materials for electron and hole transport layers in perovskite-based solar cells through SCAPS-1D simulations, in: 2016 IEEE 43rd Photovoltaic Specialists Conference (PVSC), IEEE, June, 2016, https://doi.org/10.1109/PVSC.2016.7749702 (pp. 0747-0750).

[26] O.A. Abdelraouf, N.K. Allam, Towards nanostructured perovskite solar cells with enhanced efficiency: coupled optical and electrical modeling, Sol. Energy 137 (2016) 364–370, https://doi.org/10.1016/j.solener.2016.08.039.

[27] O.A. Abdelraouf, A. Shaker, N.K. Allam, Front dielectric and back plasmonic wire grating for efficient light trapping in perovskite solar cells, Opt. Mater. 86 (2018) 311–317, https://doi.org/10.1016/j.optmat.2018.10.028.

[28] A. Tooghi, D. Fathi, M. Eskandari, "High-performance perovskite solar cell using photonic–plasmonic nanostructure.", Sci. Rep. 10 (2020) 11248, https://doi.org/10.1038/s41598-020-67741-9.

[29] O.A. Abdelraouf, A. Shaker, N.K. Allam, Novel design of plasmonic and dielectric antireflection coatings to enhance the efficiency of perovskite solar cells, Sol. Energy 174 (2018) 803–814, https://doi.org/10.1016/j.solener.2018.09.066.

[30] J.M. Ball, S.D. Stranks, M.T. Hörantner, S. Hüttner, W. Zhang, E.J. Crossland, H. J. Snaith, Optical properties and limiting photocurrent of thin-film perovskite solar cells, Energy Environ. Sci. 8 (2) (2015) 602–609, https://doi.org/10.1039/C4EE03224A.

[31] Y. Zhang, Y. Xuan, Comprehensive design of omnidirectional high-performance perovskite solar cells, Sci. Rep. 6 (2016) 29705, https://doi.org/10.1038/srep29705.

[32] O.A. Abdelraouf, N.K. Allam, Nanostructuring for enhanced absorption and carrier collection in czts-based solar cells: coupled optical and electrical modeling, Opt. Mater. 54 (2016) 84–88, https://doi.org/10.1016/j.optmat.2016.02.021.

[33] O.A. Abdelraouf, A. Shaker, N.K. Allam, All dielectric and plasmonic cross-grating metasurface for efficient perovskite solar cells, in: Metamaterials XI vol. 10671, International Society for Optics and Photonics, 2018, p. 1067120.

[34] T. Minemoto, M. Murata, Impact of work function of back contact of perovskite solar cells without hole transport material analyzed by device simulation, Curr. Appl. Phys. 14 (11) (2014) 1428–1433, https://doi.org/10.1016/j.cap.2014.08.002.

[35] O. Shunji, A. Sadao, Optical constants of cubic ZnS, Jpn. J. Appl. Phys. 32 (1993) 5008, https://doi.org/10.1143/JJAP.32.5008. IOP.

[36] A. Sadao, T. Tsunemasa, Optical properties of ZnSe, Phys. Rev. B 43 (1991) 9569, https://doi.org/10.1103/PhysRevB.43.9569. APS.

[37] S. Manzoor, J. Häusele, K.A. Bush, A.F. Palmstrom, J. Carpenter, Z.J. Yu, S.F. Bent, M.D. Mcgehee, Z.C. Holman, Optical modeling of wide-bandgap perovskite and perovskite/silicon tandem solar cells using complex refractive indices for arbitrary-bandgap perovskite absorbers, Optic Express 26 (2018) 27441–27460, https://doi.org/10.1364/OE.26.027441. Optical Society of America.

[38] S. Sarkar, V. Gupta, M. Kumar, J. Schubert, P. Probst, J. Joseph, T.A.F. Koenig, Hybridized guided-mode resonances via colloidal plasmonic self-assembled grating, ACS Appl. Mater. Interfaces 11 (2019) 13752–13760, https://doi.org/10.1021/acsami.8b20535. ACS Publications.

[39] L. Fanni, B. Delaup, B. Niesen, Y. Milstein, D. Shachal, M. Morales-Masis, S. Nicolay, C. Ballif, Tuning the porosity of zinc oxide electrodes: from dense to nanopillar films, Mater. Res. Express 2 (2015), https://doi.org/10.1088/2053-1591/2/7/075006, 075006, IOP.

[40] Z.C. Holman, M. Filipič, A. Descoeudres, S. De Wolf, F. Smole, M. Topič, C. Ballif, Infrared light management in high-efficiency silicon heterojunction and rear-passivated solar cells, J. Appl. Phys. 113 (2013), 013107, https://doi.org/10.1063/1.4772975. American Institute of Physics.

[41] Optical properties of coating materials from Sopra S.A, website, http://www.sopra sa.com, 2006.

[42] M. Filipič, P. Löper, B. Niesen, S. De Wolf, J. Krč, C. Ballif, M. Topič, CH3NH3PbI3 perovskite/silicon tandem solar cells: characterization based optical simulations, Optic Express 23 (2015) A263–A278, https://doi.org/10.1364/OE.23.00A263.

[43] G. F. Burkhard, E. T. Hoke, M. D. McGehee, "Accounting for interference, scattering, and electrode absorption to make accurate internal quantum efficiency measurements in organic and other thin solar cells." Adv. Mater., vol. 22(30), pp. 3293-3297. doi: 10.1002/adma.201000883.

[44] C.W. Chen, S.Y. Hsiao, C.Y. Chen, H.W. Kang, Z.Y. Huang, H.W. Lin, Optical properties of organometal halide perovskite thin films and general device structure design rules for perovskite single and tandem solar cells, J. Mater. Chem. 3 (2015) 9152–9159, https://doi.org/10.1039/C4TA05237D. Royal Society of Chemistry.

[45] L. Zhang, S.A. Ding, G. Qin, Efficiency simulations on perovskite solar cells only using experimentally determined reflectance and transmittance data, Sol. Energy Mater. Sol. Cell. 201 (2019) 110039, https://doi.org/10.1016/j.solmat.2019.110039.

[46] M. Burgelman, K. Decock, A. Niemegeers, J. Verschraegen, S. Degrave, SCAPS Manual, 2018. Version.

[47] X. Ziang, L. Shifeng, Q. Laixiang, P. Shuping, W. Wei, Y. Yu, Y. Minghui, Refractive index and extinction coefficient of CH3NH3PbI3 studied by spectroscopic ellipsometry, Opt. Mater. Express 5 (1) (2015) 29–43, https://doi.org/10.1364/OME.5.000029.

[48] S. Sun, X.Z. ie, G. Qin, L. Xiao, Light trapping nano structures with over 30% enhancement in perovskite solar cells, Org. Electron. 75 (2019) 105385, https://doi.org/10.1016/j.orgel.2019.105385.